HHS Public Access

Author manuscript

Nucl Med Biol. Author manuscript; available in PMC 2018 April 01.

Published in final edited form as:

Nucl Med Biol. 2017 April ; 47: 62–68. doi:10.1016/j.nucmedbio.2017.01.004.

PET Imaging of ^{64}Cu-DOTA-scFv-Anti-PSMA Lipid Nanoparticles (LNPs): Enhanced Tumor Targeting over Anti-PSMA scFv or Untargeted LNPs

Patty Wong[1], **Lin Li**[2], **Junie Chea**[2], **Melissa K. Delgado**[2], **Desiree Crow**[2], **Erasmus Poku**[2], **Barbara Szpikowska**[2], **Nicole Bowles**[2], **Divya Channappa**[2], **David Colcher**[2], **Jeffrey Y.C. Wong**[1], **John E. Shively**[2], and **Paul J. Yazaki**[2,*]

[1]Department of Radiation Oncology, City of Hope Medical Center, Duarte, CA, 91010-3000, USA

[2]Department of Molecular Immunology, Beckman Research Institute, City of Hope, Duarte, CA, 91010-3000, USA

Abstract

Introduction—Single chain (scFv) antibodies are ideal targeting ligands due to their modular structure, high antigen specificity and affinity. These monovalent ligands display rapid tumor targeting but have limitations due to their fast urinary clearance.

Methods—An anti-prostate membrane antigen (PSMA) scFv with a site-specific cysteine was expressed and evaluated in a prostate cancer xenograft model by Cu-64 PET imaging. To enhance tumor accumulation, the scFv-cys was conjugated to the co-polymer DSPE-PEG-maleimide that spontaneously assembled into a homogeneous multivalent lipid nanoparticle (LNP).

Results—The targeted LNP exhibited a 2-fold increase in tumor uptake compared to the scFv alone using two different thiol ester chemistries. The anti-PSMA scFv-LNP exhibited a 1.6 fold increase in tumor targeting over the untargeted LNP.

Conclusions—The targeted anti-PSMA scFv-LNP showed enhanced tumor accumulation over the scFv alone or the untargeted DOTA-micelle providing evidence for the development of this system for drug delivery.

Advances in Knowledge and implications for patient care—Anti-tumor scFv antibody fragments have not achieved their therapeutic potential due to their fast blood clearance. Conjugation to a LNP enables multivalency to the tumor antigen as well as increased molecular size for chemotherapy drug delivery.

*Corresponding Author. 1500 E. Duarte Road, Duarte, CA, 91010-3000, USA. Tel.: +1 626 256 4673; fax +1 626 301-8186. pyazaki@coh.org (P.J.Yazaki).

Appendix A. Supplementary Data

The Supplementary data to this article can be found online.

The authors declare no competing financial interest.

Keywords

lipid nanoparticles; polyethylene glycol; single-chain antibody; prostate cancer; positron emission tomography

INTRODUCTION

Recombinant single chain antibody (scFv) fragments retain the exquisite specificity of monoclonal antibodies [1] and their small molecular size (30 kDa) and modular nature make them attractive targeting ligands. However, few scFvs have succeeded in the clinic for cancer therapy, due to their lack of avidity and effector functions and rapid clearance from the blood circulation [2]. Modifications for improvement have included development into multivalent recombinant molecules such as diabodies, minibodies, or Fc fusions to increase valency and molecular size or the addition of polyethylene glycol (PEG) to extend serum persistence [3]. Ideally, one would like to take advantage of the ease of preparation of scFv fragments by combining them with other nanoparticles that would increase their valency (avidity), serum retention, and ability to deliver payloads such as chemotherapeutic drugs.

Lipid nanoparticles (LNP) have an extensive history as drug delivery vehicles, with more than 15 agents approved and currently over 600 clinical trials include LNPs for cancer therapy [4, 5]. Composed of a diverse set of natural or synthetic polymers, LNPs form small (10–300 nm in diameter) spherical vesicles capable of encapsulating chemotherapeutics, providing improvements over traditional systemic drug delivery [6]. Advantages to increase anti-tumor activity and decrease off target toxicity include: enhanced solubility of hydrophobic drugs, limited drug degradation by serum proteases, improved intracellular delivery by membrane fusion, and prolonged pharmacokinetics compared to small molecules. Yet many challenges remain for improvement of this drug delivery system including specific and high tumor targeting, internalization, homogenous tumor penetration, formulation of multiple drug payloads, quantitation of tumor vs. normal tissue uptake, and reduction of toxicity.

The use of targeted LNPs has had mixed results for tumor accumulation over what can be achieved by untargeted LNPs through the passive enhanced permeability retention (EPR) effect [7]. The generation of targeted LNPs has been widely attempted but with varying results due to limitations of the ligand-receptor or antigen-antibody system selected and the resulting LNP molecular size [8].

LNPs fall roughly into two categories, liposomes and micelles. The use of targeted liposomes for drug delivery has an extensive literature, but on the whole, performs no better than untargeted liposomes due to their rather large molecular size (50–200 nm) [9, 10]. Micelles have a smaller molecular size (10–20 nm), are formed by the self assembly of lipid hydrophilic and hydrophobic domains and have many attractive features, including high water solubility and rapid diffusion into the tumor vascular bed [11]. The amphipathic block co-polymer, distearoyl phosphatidyl ethanolamine monomethoxy polyethylene glycol (DSPE-PEG) has been the mainstay for the synthesis of micelle drug delivery [11]. Immuno-

targeted micelles have demonstrated increased accumulation at the tumor site due to their smaller molecular size [12].

Given the attraction of a self-assembled micelle over the rather tedious preparation of liposomes, we have selected DSPE-PEG micelles for evaluating targeted LNPs. In this study, we show that an scFv can be covalently attached to DSPE-PEG LNP conferring improved anti-tumor targeting compared to an unconjugated scFv fragment or an untargeted LNP.

Radionuclide imaging has shown the ability to track *in vivo* liposomal formulations to provide pharmacokinetic and pharmacodynamic data [13]. In this study, Cu-64 PET imaging is used for quantitative *in vivo* analysis of tumor vs. normal tissue uptake to evaluate the performance of the targeted vs. untargeted micelle LNP.

We have selected prostate cancer as a model system, given its clinical significance as a major cause of cancer mortality in men[14]. In this disease, prostate specific membrane antigen (PSMA) is a key biomarker for prostate cancer, in which its overexpression correlates with metastatic and advanced prostate cancer [12] [15]. An anti-PSMA scFv antibody fragment was developed based on the anti-PSMA J591 monoclonal antibody with a site-specific cysteine (cys) for thiol conjugation[15–18]. In this report we evaluate radiolabeled ^{64}Cu-DOTA anti-PSMA scFv-cys fragment alone and its conjugate to DSPE PEG-free thiol LNP by PET imaging, together with biodistribution studies in a mouse xenograft model.

MATERIAL AND METHODS

anti-PSMA scFv-cys

An anti-PSMA scFv antibody based on the anti-human PSMA monoclonal antibody J591[19] was constructed in the V_H-V_L orientation joined by a glycine/serine (G/S) 16 amino acid linker, L6 linker [20], six histidine tag, G/S 5 amino acid linker and a carboxy-terminal cys (Figure 1A). The cDNA encoding the scFv-cys was cloned into the pEE12.4 plasmid (Lonza Group Ltd, Basil, Switzerland) and transiently expressed using the Expi293™ Expression system (Life Technologies, Grand Island, NY). The culture supernatants were affinity purified on Ni-NTA superflow cartridge following the manufacture's method (Qiagen, Germantown, MD). The scFv-cys was further purified by ceramic hydroxyapatite, Type I (Biorad Laboratories, Hercules, CA) [21]

DOTA-anti-PSMA scFv-cys

For radiometal labeling, the anti-PSMA scFv-cys was conjugated with the metal chelate, *N*-hydroxysuccinimide - 1,4,7,10-tetraazacyclododecane- 1, 4, 7, 10 tetraacetic acid (NHS-DOTA) (Macrocyclics, Dallas, TX, Cat. No. B280) as previously described [22]. Briefly, the anti-PSMA scFv-cys (952 μL of 2.1 mg/mL in PBS) was reacted with a 30-molar excess of DOTA-NHS for 24 h at RT and dialyzed vs. PBS to remove excess free DOTA. DOTA-anti-PSMA scFv-cys was analyzed by IEF gel electrophoresis. The downward shift of the scFv-cys protein isoform bands to a more acidic pH is indicative of conjugation of the acidic DOTA chelate (Figure S1).

DOTA-anti-PSMA scFv-cys-mal-LNP

The DOTA-anti-PSMA scFv-cys (160 μL of 2.28 mg/mL, 14.56 nmoles in PBS) was reduced with a 10-molar excess (21 μL of 20 mM) Tris (2-carboxyethyl) phosphine (TCEP) at 37°C for 2 h under argon gas. TCEP was removed using a desalting spin column (Zeba, 7 kDa mwt. cutoff, Thermo Scientific). DSPE-PEG_{2000}-mal (171 μL of 2.58 mg/mL, 14.56 nmole in PBS, (Avanti Polar Lipids, Inc., Alabaster, AL, Cat. No. 880126) was reacted overnight with TCEP reduced DOTA-scFv-cys at 37°C under argon. The product, DOTA-anti-PSMA scFv-cys-mal-LNP was analyzed by size exclusion chromatography (SEC)-HPLC (Superdex 200 10/300 column; GE Healthcare) as previously described [23]. The post-conjugation chromatograms are shown before and after purification (Figure S2A) and by scanning electron microscopy (SEM) (Figure S2B and C).

DOTA-anti-PSMA-scFv-cys-acetBr-LNP

DSPE-PEG_{2000}-NH_2 (6 mg in 300 μL of DCM) was reacted with a 10-molar excess of bromoacetyl bromide (acetBr) with a 10 molar excess of triethylamine (TEA). The product was evaporated to dryness and the product confirmed by ESI-MS (data not shown). Reduced DOTA-scFv-cys (0.364 mg in 146 μL of PBS) was reacted with an 11.5-molar excess of DSPE-PEG_{2000}-acetBr (0.5 mg in 99 μL of PBS) overnight at 37°C. The DOTA-anti-PSMA-scFv-cys-acetBr-LNP product analyzed by SEC-HPLC and SEM as above, offered equivalent results to those obtained for the maleimide product (data not shown).

DOTA-LNP

A solution of DOTA-NHS-ester (209 mg in 1 mL of water) was mixed with a 1.5-molar excess of 1-amino-2-thiol-ethane (31.7 mg), the pH adjusted to 7.0 and reacted for 24 h at RT. The product purified by ion exchange chromatography (Bio-Rad 140-1454 AG 1x XB, eluted with 4M formic acid) gave the expected mass by ESI-MS (M+H of 464.21 predicted, 464.22 observed). DOTA-monoacetamidoethanethiol (5.4 μL of 5.3 mg in 400 μL of water) was mixed with a solution of DSPE-PEG_{2000}-mal (2.5 mg of DSPE-PEG_{2000}-mal in 392 μL of water, 182 μL) the pH adjusted to 7.3 and reacted for 2 h at RT under argon. Excess DOTA-monoacetamidoethanethiol was removed by a spin column and the product analyzed by ESI-MS (Figure S4). A series of z=2 peaks were obtained for DSPE-PEG_{2000}-mal differing by 22 mass units that correspond to the expected masses of the polymeric series where m/z=1 of 2941 is the reported mass for n=45 PEG units (Avanti, Cas No. 474922-22-0), while the corresponding series for DOTA-monoacetamidoethanethiol plus Na + (m+Na)= 483) plus the DSPE-PEG_{2000}-mal Michael addition product. For SEC analysis, a major micelle peak at 17.65 min was observed for the DOTA-LNP with a minor peak at 39.96 min corresponding to residual DOTA-monoacetamidoethanethiol (Figure S5). DOTA-acetamidoethanethiol-DSPE-PE_{G2000}-acetBr was similarly prepared, purified and characterized (data not shown).

Electron microscopy

Electron microscopy was performed on an FEI Tecnai 12 transmission electron microscope equipped with a Gatan Ultrascan 2K CCD camera. LNP samples were applied to a glow-

discharged 300 mesh Formvar-carbon copper EM grid and stained with 2% uranyl acetate or Nano-W®.

Radiolabeling

The DOTA-anti-PSMA-scFv-cys, DOTA-anti-PSMA-acetBr-LNP, DOTA-anti-PSMA-mal-LNP and DOTA-LNP were radiolabeled with Cu-64 to a specific activity of ~0.37MBq per μg as previously described [24]. Briefly, the DOTA-constructs were adjusted to 0.25M ammonium acetate pH 5.5, incubated with ^{64}Cu chloride (Isotope Production group, Washington University Medical School in St. Louis, St Louis, MO) at 43°C for 45 min, adjusted to 1 mM DTPA and incubated for 10 min at room temperature. Radiolabel incorporation was greater than 75% as measured by instant thin layer chromatography. The ^{64}Cu-DOTA-constructs were purified on a SEC Superdex 200 column immediately before injection into animals.

The ^{64}Cu-DOTA-anti-PSMA scFv constructs were analyzed for immunoreactivity by co-incubation with soluble PSMA-Fc (R&D Systems, Minneapolis, MN). In a liquid phase assay radiolabeled immmuno-LNPs were incubated with 20 equivalents by mass of antigen and the resultant complex analyzed by analytical HPLC-SEC. The immunoreactivity was determined by integrating the area on the HPLC radiochromatogram and calculating the percentage of radioactivity shifting to higher molecular weight, consistent with the complexation of the immune-LNP with its cognate antigen.

Animal biodistribution and PET imaging studies in tumor-bearing mice

All animal handling was done in accordance with protocols approved by the City of Hope Institutional Animal Care and Use Committee. Male NOD SCID mice were injected in the preputial fat pad with mixture of Matrigel (Thermo Fisher Scientific, Waltham, MA) and LNCaP prostate cancer cells (#CRL-1740, ATCC Manassas, VA) at a ratio of 7:3, v/v. After 4–8 weeks, the tumor masses were in the range of 0.2–0.6 g. In individual experiments, ^{64}Cu-DOTA-anti-PSMA-scFv-cys, ^{64}Cu-DOTA-anti-PSMA-Br-LNP, ^{64}Cu-DOTA-anti-PSMA-mal-LNP, ^{64}Cu-DOTA-acetBr-LNP and ^{64}Cu-DOTA-mal-LNP were injected (3.7 MBq/animal) via tail vein with two mice per group. The PET imaging was performed at set time points using a Siemens InVeon microPET system. At the last time point, CT imaging was performed when available, the CT and PET images were aligned for co-registration.

After the final images were taken, the mice were euthanized, necropsy performed, organs weighed and counted for radioactivity. The radioactivity has been corrected for background and radioactive decay from the time of injection, allowing organ uptake to be reported as % ID/g.

RESULTS and DISCUSSION

Anti-PSMA scFv-cys antibody

An anti-PSMA single scFv-cys antibody fragment was genetically engineered from the genes encoding the variable light and heavy chains of the murine anti-PSMA J591

monoclonal antibody [3]. The scFv was designed with a six histidine amino acid sequence for purification and a site-specific C-terminal cys for thiol conjugation chemistry (Figure 1A). The anti-PSMA scFv-cys antibody was produced in a transient mammalian expression system that yielded 40–60 μg/ml under non-optimized conditions. The scFv-cys was purified to homogeneity by immobilized metal affinity chromatography [25] and ceramic hydroxyapatite chromatography [21]. Molecular size analysis by SDS-PAGE showed the scFv-cys was a single band under non-reducing and reducing conditions (Figure 1B). Analysis by size exclusion chromatography (SEC) showed the purified scFv-cys was an equal mixture of monomer and non-covalent dimer (Figure 1C).

For Cu-64 PET imaging, the anti-PSMA scFv-cys was conjugated by amine chemistry with the metal chelate, NHS-DOTA. After test radiolabeling, the ^{64}Cu-DOTA-anti-PSMA scFv-cys antibody exhibited 100% binding to a soluble form of recombinant PSMA antigen as shown by a complete molecular size shift by SEC analysis (Figure 1D).

LNP synthesis—To enhance tumor targeting of the monovalent, low molecular weight scFv-cys, the scFv-cys was conjugated to the phospholipid block co-polymer DSPE-PEG_{2000} by an active thiol group to increase its multivalency and extend serum persistence. Two different thiol ester-PEG chemistries were tested for attachment of the antibody, DSPE-PEG_{2000}-maleimide (mal) and DSPE-PEG_{2000}-acetamidobromomide (acetBr). As an overview of the LNP constructs, a schematic representation is shown in Figure 2. The DSPE-PEG_{2000}-mal is commercially available and has a long history for the synthesis of targeted liposomal delivery agents [26]. However based on reports of instability of the maleimidocysteineamido linkage at physiological pH [27], we also synthesized an acetBr derivative by reacting DSPE-PEG_{2000}-NH_2 with bromoacetyl bromide. The DOTA-anti-PSMA scFv-cys was reduced with TCEP and reacted with the DSPE-PEG_{2000}-mal or DSPE-PEG_{2000}-acetBr at a molar ratio of 1:4 (antibody: LNP). The scFv-LNPs were purified by HPLC SEC and the purified micelles shown to have an average size of 12 nm by transmission electron microscopy (Figure S2), similar to the size of unconjugated DSPE-PEG_{2000} LNPs [28]. Untargeted DOTA-LNPs were produced in a similar manner, using DOTA-monoacetamidoethanethiol (reacted with the DSPE-PEG_{2000}-acetBr, Figure S3) or DSPE-PEG_{2000}-mal (Figure 2). The untargeted LNP was used as a control as this represents the majority of micelle reported in the literature. An additional control may have been a non-targeted scFv-LNP but was unavailable at the time of the study.

PET imaging

In individual experiments, the DOTA-anti-PSMA-scFv-cys antibody, DOTA-mal-LNP, DOTA-acetBr-LNP, DOTA anti-PSMA scFv-mal-LNP and DOTA-anti-PSMA scFv-acetBr-LNP were radiolabeled with ^{64}Cu and purified by SEC. The purified ^{64}Cu-DOTA-scFv-cys or LNPs were administered by tail vein injection into NOD/SCID mice bearing human prostate cancer LNCap tumors. Positron Emission Tomography (PET) serial images were acquired for two mice per group at three time points to determine tumor targeting, blood clearance and tissue biodistribution. For most constructs, the imaging study was repeated and the tissue biodistribution data averaged (n=2–4 mice). Maximum intensity projections (MIP) images were generated and each panel of serial images normalized for comparison.

To aid in tissue registration, the last image for most of the series included co-registration of a computer tomography (CT) image. Representative PET images of the various LNP constructs are displayed in Figure 3. To establish a baseline for the scFv-cys antibody fragment, PET images were acquired of the ^{64}Cu-DOTA-anti-PSMA scFv-cys at 0.5 h, 1 h, and 4 h. The PET images show the 30 kDa scFv-cys had the expected rapid clearance from the circulation through the urinary system, with only the kidneys, bladder and tumor visible at the 4 hour terminal time point (Figure 3A).

The untargeted LNPs, ^{64}Cu-DOTA-mal-LNP and ^{64}Cu-DOTA-acetBr-LNP DOTA-LNP, displayed predominantly liver uptake, with slow clearance over the 2 day time course (4 h, 20–23 h, 43–46 h) as shown for the ^{64}Cu-DOTA-acetBr-LNP in Figure 3B. The early localization to the liver was anticipated due to clearance of the ~10–20 nm micelles by the reticuloendothelial system[11]. For the targeted LNP, anti-PSMA scFv-cys-mal-LNP and anti-PSMA scFv-cys-acetBr-LNP, accumulation of radioactivity was observed in the liver, kidney, spleen, bladder and tumor vs. only kidney and tumor for the scFv-cys at the 4 h image acquisition. Clearance from the blood was observed over the two-day time course. The 2-day PET images showed accumulation of activity in the tumor with residual amounts in the liver (Figure 3C and 3D, respectively).

Immediately after the last PET images were acquired, the mice were euthanized, tissues weighed and counted for radioactivity. The tissue biodistribution data are reported as the percent injected dose per gram (% ID/g) for each mouse (Figure 4). The tumor, liver and kidney % ID/g for the specific mice that were imaged are displayed on the image for the final time point (Figure 3). The PET images agreed with the terminal biodistribution data for the untargeted or targeted LNPs to the major organs showing accumulation in the liver, spleen, kidney and tumor.

Importantly, the conjugation of the scFv-cys to the LNP resulted in two-fold increase of tumor uptake compared to the scFv-cys alone (averaged 10% ID/g vs. 4.8% ID/g, respectively). The biodistribution data showed the targeted anti-PSMA-LNPs had a 60% increase in tumor uptake compared to the non-targeted LNP (averaged 10.4% ID/g versus 6.5% ID/g, respectively). Thus, the targeting of LNP provides a clear advantage over non-targeted LNP in this anti-PSMA prostate cancer model, a result not observed for many antibody-receptor xenograft models [27].

No clear differences in tumor targeting were observed due to the different thiol conjugation chemistries. The anti-PSMA-LNP acetBr and mal derivatives had a tumor uptake of 11.4% ID/g and 9.3% ID/g, respectively. While there were differences in liver and kidney uptake, it did not dramatically change the tumor accumulation. Similarly, the untargeted acetBr and mal DOTA-LNPs showed no major difference in tumor activity with the averaged value of 6.9% ID/g and 6.0% ID/g, respectively at the terminal time point. Presumably the rather significant untargeted LNP tumor accumulation is due to the EPR effect [29]. Targeted versus non-targeted LNPs had similar blood clearance rates, lowering to approximately 2–4% ID/g over the two-day time period (Figure 3).

Time activity curves were determined for the serial PET images (Figure S6). Regions of Interest were drawn for heart, liver, kidney and tumor at the 3 serial time points for each construct and quantified as % ID/g based on the activity obtained at the terminal biodistribution. The curves show clearance of the radiolabeled LNP from the blood based on the activity in the heart, with slower clearance from the liver. Differing from the terminal biodistribution data, there was significant kidney activity at the initial time point for the ^{64}Cu-DOTA-anti-PSMA scFv-acetBr-LNP, indicating the loss of some portion of the ^{64}Cu-DOTA-anti-PSMA-scFv.

An interesting observation was that the non-targeted LNP had a higher tumor accumulation than the free anti-PSMA scFv-cys antibody at the different terminal time periods (averaged 6.5% ID/g at 44 h vs. 4.8% ID/g at 4 h, respectively). Thus, the EPR effect for an untargeted LNP vs. targeted scFv over a longer circulation time can yield higher tumor accumulation than the specific targeting of the small rapidly clearing antibody fragment. These data provide a likely rationale for the popularity of untargeted liposomal formulations for drug delivery. However, this effect can be further improved by the proper choice of an additional targeting agent conjugated to the LNP, as shown in our current study.

CONCLUSION

In this report, we produced an anti-PSMA scFv-cys antibody fragment to determine if site-specific conjugation to a LNP would increase solid tumor accumulation by enhanced valency, avidity or retention due to multiple scFv per LNP and extension of persistence in the circulation due to the molecular size of the scFv-LNP vs. free scFv. In a human prostate cancer xenograft model, the ^{64}Cu-DOTA scFv-LNP showed a 2-fold increase in tumor uptake compared to the ^{64}Cu-DOTA scFv-cys as determined by ^{64}Cu-PET imaging and radioactive tissue biodistribution studies. Two different thiol conjugation chemistries were used for the synthesis of targeted anti-PSMA and untargeted LNPs, but showed no significant difference in tumor uptake suggesting that the reported instability of the maleimide linker at physiological pH played a minimal role in decreasing tumor uptake. While the liver and kidney activities varied for the two thiol chemistries, for this limited pilot study it is unknown if the linking chemistries have an effect on the stability of the LNP.

Importantly, the targeted anti-PSMA LNP showed a 60% increase in tumor accumulation over the DOTA-micelle providing evidence for the development of this system for drug delivery. Presumably this increase is due to targeting to the tumor surface antigen but alternative postulates can be enhanced retention in the tumor, or modification of cellular clearance mechanisms. Optimization of the antibody construct, site of attachment and chemical synthesis of novel LNPs are under development toward higher efficiency of coupling, ligand density and tumor targeting. This study is only first step in our development of “smart” targeted LNPs where multiple ligands are attached for radioactive and optical imaging, as well a therapeutic drug delivery.

Supplementary Material

Refer to Web version on PubMed Central for supplementary material.

Acknowledgments

We wish to thank the City of Hope Electron Microscope Core Facility, whose use of the FEI Tecnai 12 transmission electron microscope was provided by Office of Naval Research N00014-02-1 0958.

Research reported in this publication included work performed in the Small Animal Imaging Core supported by the National Cancer Institute of the National Institutes of Health under award number P30CA33572. The content is solely the responsibility of the authors and does not necessarily represent the official views of the National Institutes of Health.

Support from the Charles Reames Family (to J.W.) is gratefully acknowledged.

ABBREVIATIONS

scFv	single chain antibody
PEG	polyethylene glycol
LNP	Lipid nanoparticles
EPR	enhanced permeability retention
DSPE-PEG	distearoyl phosphatidyl ethanolamine monomethoxy polyethylene glycol
PSMA	prostate specific membrane antigen
His_6	six histidine
cys	cysteine
IMAC	immobilized metal affinity chromatography
HPLC	high performance liquid chromatography
SEC	size exclusion chromatography
NR	non-reducing
DOTA	1,4,7,10-tetraazacyclododecane-1, 4,7,10-tetraacetic acid
NHS	*N*-hydroxysuccinimide
r	recombinant
acetBr	acetamidobromomide
mal	maleimide
PET	positron emission tomography
MIP	maximum intensity projections
CT	computed tomography
% ID/g	percent injected dose per gram

REFERENCES

1. Ahmad ZA, et al. scFv antibody: principles and clinical application. Clin Dev Immunol. 2012; 2012:980250. [PubMed: 22474489]
2. Nelson AL. Antibody fragments: hope and hype. MAbs. 2010; 2(1):77–83. [PubMed: 20093855]
3. Holliger P, Hudson PJ. Engineered antibody fragments and the rise of single domains. Nat Biotechnol. 2005; 23(9):1126–1136. [PubMed: 16151406]
4. Kraft JC, et al. Emerging research and clinical development trends of liposome and lipid nanoparticle drug delivery systems. J Pharm Sci. 2014; 103(1):29–52. [PubMed: 24338748]
5. Musacchio T, Torchilin VP. Recent developments in lipid-based pharmaceutical nanocarriers. Front Biosci (Landmark Ed). 2011; 16:1388–1412. [PubMed: 21196238]
6. Torchilin VP. Multifunctional, stimuli-sensitive nanoparticulate systems for drug delivery. Nat Rev Drug Discov. 2014; 13(11):813–827. [PubMed: 25287120]
7. Maeda H. Tumor-selective delivery of macromolecular drugs via the EPR effect: background and future prospects. Bioconjug Chem. 2010; 21(5):797–802. [PubMed: 20397686]
8. Wittrup KD, et al. Practical theoretic guidance for the design of tumor-targeting agents. Methods Enzymol. 2012; 503:255–268. [PubMed: 22230572]
9. Schmidt MM, Wittrup KD. A modeling analysis of the effects of molecular size and binding affinity on tumor targeting. Mol Cancer Ther. 2009; 8(10):2861–2871. [PubMed: 19825804]
10. Kirpotin DB, et al. Antibody targeting of long-circulating lipidic nanoparticles does not increase tumor localization but does increase internalization in animal models. Cancer Res. 2006; 66(13): 6732–6740. [PubMed: 16818648]
11. Torchilin VP. Micellar nanocarriers: pharmaceutical perspectives. Pharm Res. 2007; 24(1):1–16. [PubMed: 17109211]
12. Ristau BT, O'Keefe DS, Bacich DJ. The prostate-specific membrane antigen: lessons and current clinical implications from 20 years of research. Urol Oncol. 2014; 32(3):272–279. [PubMed: 24321253]
13. van der Geest T, et al. Radionuclide imaging of liposomal drug delivery. Expert Opin Drug Deliv. 2016; 13(9):1231–1242. [PubMed: 27351233]
14. Siegel RL, Miller KD, Jemal A. Cancer statistics, 2015. CA Cancer J Clin. 2015; 65(1):5–29. [PubMed: 25559415]
15. Barve A, Jin W, Cheng K. Prostate cancer relevant antigens and enzymes for targeted drug delivery. J Control Release. 2014; 187:118–132. [PubMed: 24878184]
16. Bander NH, et al. Targeting metastatic prostate cancer with radiolabeled monoclonal antibody J591 to the extracellular domain of prostate specific membrane antigen. J Urol. 2003; 170(5):1717–1721. [PubMed: 14532761]
17. Bander NH, et al. Phase I trial of 177lutetium-labeled J591, a monoclonal antibody to prostate-specific membrane antigen, in patients with androgen-independent prostate cancer. J Clin Oncol. 2005; 23(21):4591–4601. [PubMed: 15837970]
18. Liu H, et al. Monoclonal antibodies to the extracellular domain of prostate-specific membrane antigen also react with tumor vascular endothelium. Cancer Res. 1997; 57(17):3629–3634. [PubMed: 9288760]
19. Smith-Jones PM, et al. In vitro characterization of radiolabeled monoclonal antibodies specific for the extracellular domain of prostate-specific membrane antigen. Cancer Res. 2000; 60(18):5237–5243. [PubMed: 11016653]
20. Le Gall F, et al. Effect of linker sequences between the antibody variable domains on the formation, stability and biological activity of a bispecific tandem diabody. Protein Eng Des Sel. 2004; 17(4):357–366. [PubMed: 15126676]
21. Yazaki PJ, Clark C, Shively L, Cheung C-w, Le W, Szpikowska B, Shively JE, Raubitschek AA, Wu AM. Mammalian expression and hollow fiber bioreactor production of recombinant anti-CEA diabody and minibody for clinical applications. J. Immunological Methods. 2001; 253:195–208. [PubMed: 11384681]

22. Lewis MR, et al. An improved method for conjugating monoclonal antibodies with N-hydroxysulfosuccinimidyl DOTA. Bioconjug Chem. 2001; 12(2):320–324. [PubMed: 11312695]
23. Yazaki PJ, Wu AM. Expression of recombinant antibodies in mammalian cell lines. Methods Mol Biol. 2004; 248:255–268. [PubMed: 14970502]
24. Mortimer JE, et al. Functional imaging of human epidermal growth factor receptor 2-positive metastatic breast cancer using (64)Cu-DOTA-trastuzumab PET. J Nucl Med. 2014; 55(1):23–29. [PubMed: 24337604]
25. Cheung RC, Wong JH, Ng TB. Immobilized metal ion affinity chromatography: a review on its applications. Appl Microbiol Biotechnol. 2012; 96(6):1411–1420. [PubMed: 23099912]
26. Marques-Gallego P, de Kroon AI. Ligation strategies for targeting liposomal nanocarriers. Biomed Res Int. 2014; 2014:129458. [PubMed: 25126543]
27. Lewis MR, Shively JE. Maleimidocysteineamido-DOTA derivatives: new reagents for radiometal chelate conjugation to antibody sulfhydryl groups undergo pH-dependent cleavage reactions. Bioconjug Chem. 1998; 9(1):72–86. [PubMed: 9460549]
28. Sawant RR, Torchilin VP. Polymeric micelles: polyethylene glycol-phosphatidylethanolamine (PEG-PE)-based micelles as an example. Methods Mol Biol. 2010; 624:131–149. [PubMed: 20217593]
29. Cerqueira BB, et al. Nanoparticle therapeutics: Technologies and methods for overcoming cancer. Eur J Pharm Biopharm. 2015; 97(Pt A):140–151. [PubMed: 26515260]

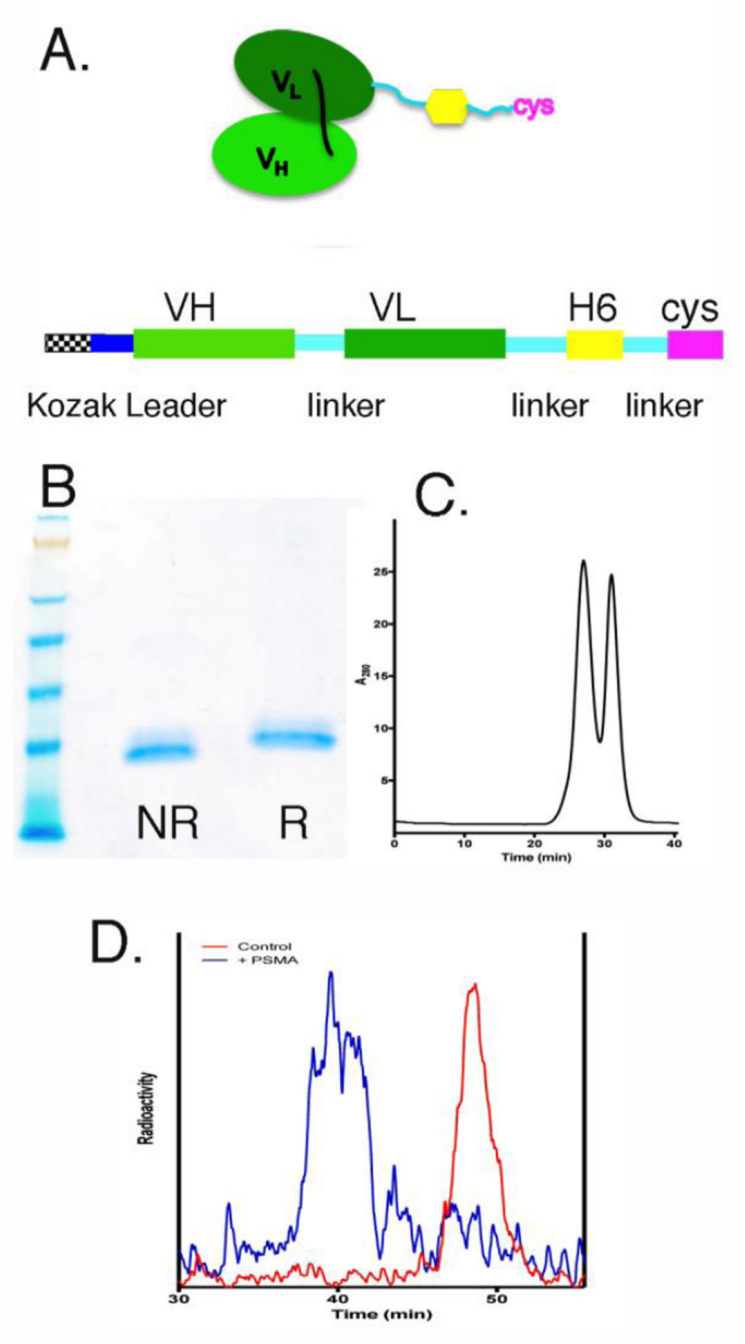

Figure 1.

Biochemical analysis of anti-PSMA scFv-cys. (**A**) Schematic of anti-PSMA scFv-histidine-6-cysteine antibody structure and cDNA gene construction. (**B**) SDS gel electrophoresis of purified scFv-Cys under non-reducing (NR) and reducing (R) conditions and with coomassie staining. (**C**) Superdex 75 SEC analysis of purified scFv-cys antibody. (**D**) Immunoreactivity assay of purified ^{64}Cu-DOTA-anti-PSMA-scFv-cys antibody (red) incubated with 20x molar excess of recombinant PSMA antigen (blue).

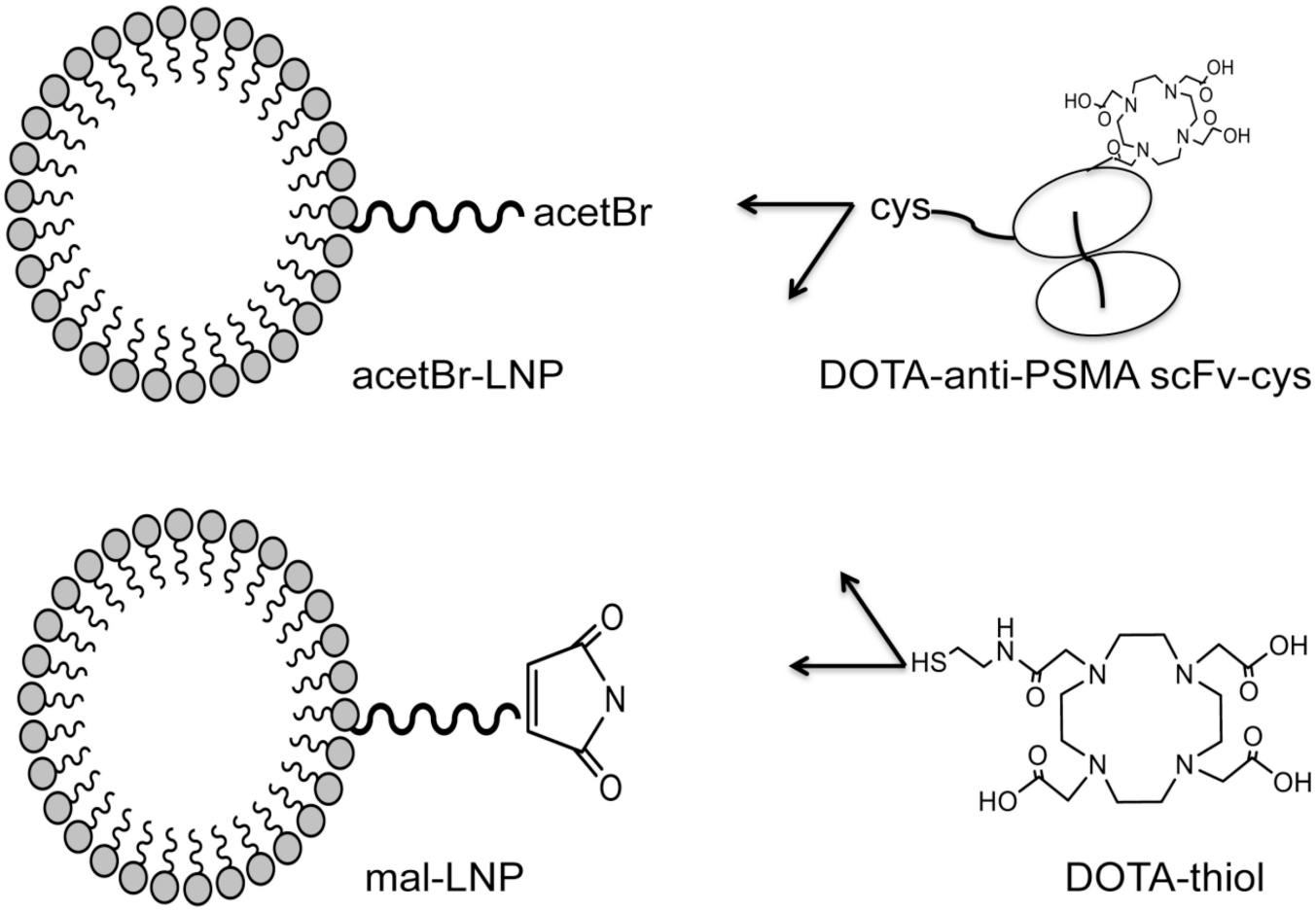

Figure 2.

Schematic diagram of LNP constructs. DSPE-PEG_{2000}-acetBr (acetBr-LNP) and DSPE-PEG_{2000}-maleimide (mal-LNP) were conjugated to the DOTA-anti-PSMA scFv-cys or DOTA-monoacetamidoethanethiol (DOTA-thiol).

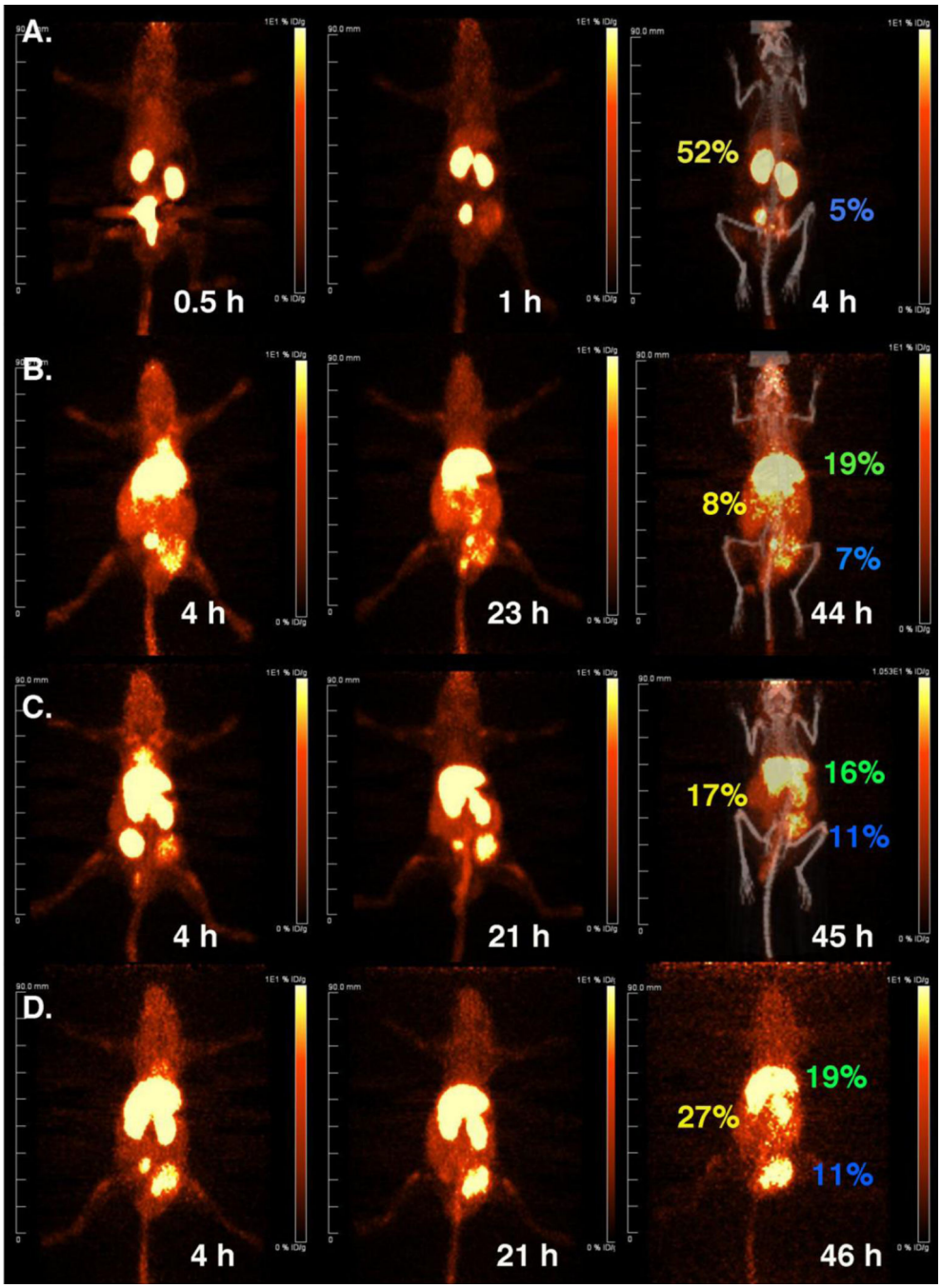

Figure 3.

Dynamic PET imaging of ^{64}Cu-DOTA-anti-PSMA scFv-cys, ^{64}Cu-DOTA-untargeted and targeted LNP in NOD-SCID mice bearing PSMA positive LNCap prostate tumors. (**A**) ^{64}Cu-DOTA-anti-PSMA-scFv-cys; (**B**) ^{64}Cu-DOTA-LNP; (**C**) ^{64}Cu-DOTA-anti-PSMA scFv-cys-mal-LNP; (**D**) ^{64}Cu-DOTA-anti-PSMA-scFv-cys-acetBr-LNP. Images are PET anterior-view maximum intensity projections (MIP) normalized to reflect radioactive decay-corrected relative image per unit injected activity. Labels in yellow, green and blue show directly measured %ID/g in kidney, liver and tumor, respectively.

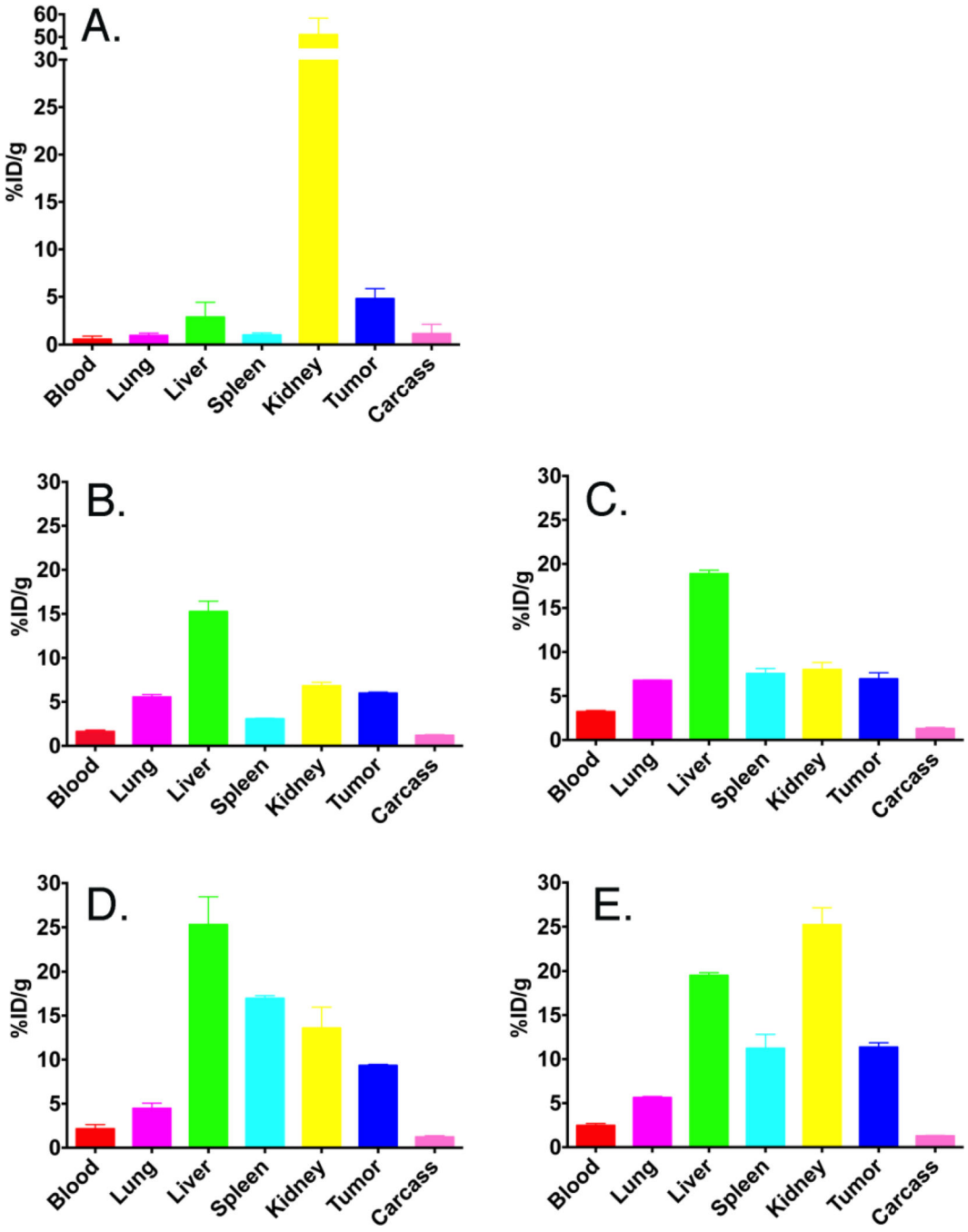

Figure 4.

Biodistributions of ^{64}Cu-DOTA-anti-PSMA-scFv-cys versus untargeted ^{64}Cu-DOTA-LNP or ^{64}Cu-DOTA-anti-PSMA-scFv-cys-LNP in NOD-SCID mice bearing PSMA positive LNCap prostate tumors at terminal time point. The average % ID/g of 2–4 animals per terminal time point (4h for scFv-cys and 43–46 h for LNPs) is shown. (**A**) ^{64}Cu-DOTA-anti-PSMA-scFv-cys; (**B**) ^{64}Cu-DOTA-mal-LNP; (**C**) ^{64}Cu-DOTA-acetBr-LNP; (**D**) ^{64}Cu-DOTA-anti-PSMA scFv-mal-LNP; (**E**) ^{64}Cu-DOTA-anti-PSMA scFv-acetBr-LNP.